# Study of cosmic charged particle events with the PolarquEEEst experiment

H. Alida F. Hardersen
(Dated: April 30, 2020)

## I. COSMIC RAYS

The cosmic rays were first discovered by Victor Hess in 1912 by using a balloon to measure radiation in the atmosphere at different altitudes, both on normal days and once during a near-total eclipse. Because the ionization remained the same in both cases he concluded that the radiation could not come from the sun, and thus had discovered another natural source of high-energy particles. His discoveries were confirmed by Werner Kolhörster in 1914, and the term *Cosmic Rays* was coined by Robert Millikan and Harvey Cameron in an article in 1926. There have been numerous experiments dedicated to cosmic rays through history, which have led to discoveries such as the positron, muon and kaon.

The particles accelerated to high energies by astrophysical sources are called *primary* cosmic rays. These particles mainly originate from sources outside our solar system and consists of stable charged particles and nuclei with lifetimes of the order of $10^6$ years or longer to survive the journey through space. The energies of primary cosmic rays are between 1 GeV and $10^8$ TeV and the rate of these particles arriving at the top of the atmosphere decreases with increasing energy as shown in figure 1. The particles produced when the primary cosmic rays interact with interstellar gas are called *secondary* cosmic rays. About 70% of the primary particles are free protons and about 70% of the rest is helium nuclei[1].

Primary cosmic rays can be measured directly by experiments in space( PAMELA, Fermi, AMS-02 and DAMPE experiments) or by balloons placed in the atmosphere where there is sufficient flux. When the primary rays hit the atmosphere, they interact and generate showers of secondary particles(mostly muons) which can be detected in the atmosphere, at the earth's surface(Icecube, Auger), or underground.

## II. THE POLA DETECTORS

When a charged particle passes through the plastic scintillators it produces a light that is converted to an electric pulse signal by the silicon photomultipliers. The signals are then sent to eight front-end boards where only signals above a certain threshold are selected.

## III. DATA ANALYSIS

### A. Environmental Conditions

The indoor- and outdoor temperature and pressure over time for POLA-01 is shown in FIG.2a. The indoor

and outdoor temperature follows the same curve, with
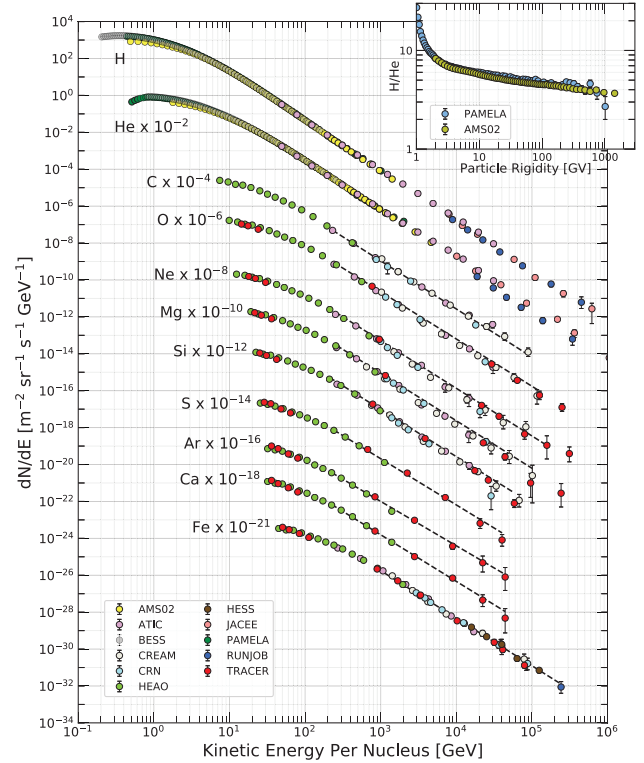


**FIG. 1:** Plot from Review of Particle physics [1]. Fluxes of nuclei of the primary cosmic radiation in particles per energy-per-nucleus are plotted vs energy-per-nucleus

indoor temperature slightly higher(average difference between indoor and outdoor is 1.6°C). Over the whole time period the indoor temperature ranges between a minimum of 17.4°C (13/08/18) and a maximum of 32.9°C (03/09/18) and the average indoor temperature is 25.4°C. The outdoor temperature has a minimum of 15.9°C (13/08/18) and a maximum of 31.2°C (03/09/18) and average 23.75°C. The pressure has a maximum value of 1030.8 mbar (31/08/18) and a minimum value of 986.7 mbar (18/08/18). The average pressure over the whole time period is 1012.6 mbar.

The temperatures and pressure for POLA-02 and POLA-03 are illustrated in FIG.2b and FIG. 2c respectively. The indoor temperature is in both cases ∼ 1°C higher than the outdoor temperature, and the difference between minimum and maximum temperature is ∼ 1° C for POLA-02 and ∼ 7.5°C for POLA-03, both in the case of indoor and outdor temperatures. The actual values are given in TAB. I.

POLA-01 is located on a sailboat, while POLA-02 and POLA-03 are located in high scools in Norway and Italy respectively. This may be the reason for the more stable temperatures in the selected time period.

**TABLE I:** Maximum, minimum, average and difference(|maximum-minimum|) in temperatures and pressure for all three detectors.

| Name | Variable | Maximum | Minimum | Average | Difference |
|------|----------|---------|---------|---------|------------|
| | Indoor Temperature [°C] | 32.89 (2018-09-03) | 17.34 (2018-08-13) | 25.39 | 15.55 |
| POLA-01 | Outdoor Temperature [°C] | 31.17 (2018-09-03) | 15.98 (2018-08-13) | 23.75 | 15.19 |
| | Pressure [mbar] | 1030.79(2018-08-31) | 986.75 (2018-08-18) | 1012.62 | 44.04 |
| | Indoor Temperature [°C] | 25.50 (2018-08-24) | 24.64(2018-07-22) | 25.06 | 0.86 |
| POLA-02 | Outdoor Temperature [°C] | 24.45 (2018-08-10) | 23.73 (2018-08-05) | 24.13 | 0.73 |
| | Pressure [mbar] | 1023.75 (2018-09-02) | 991.33 (2018-08-24) | 1008.56 | 32.41 |
| | Indoor Temperature [°C] | 36.76 (2018-08-04) | 29.10 (2018-08-01) | 33.37 | 7.66 |
| POLA-03 | Outdoor Temperature [°C] | 37.94 (2018-08-04) | 30.62 (2018-08-01) | 34.67 | 7.31 |
| | Pressure [mbar] | 990.96 (2018-08-10) | 975.79 (2018-07-22) | 985.96 | 15.17 |
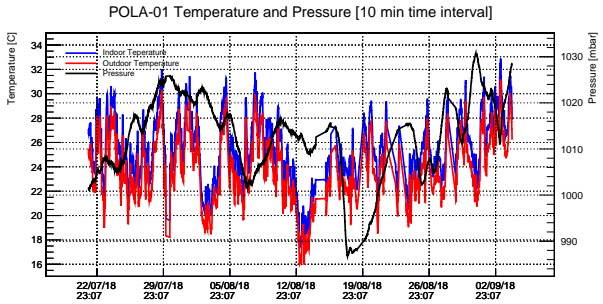


**(a)** POLA-01
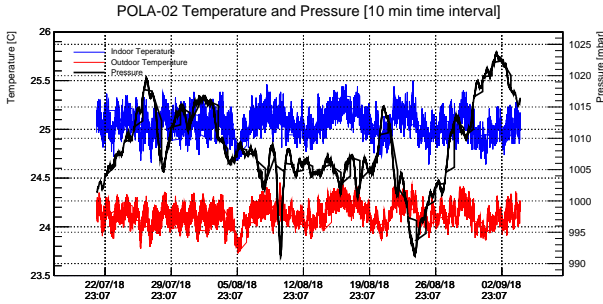


**(b)** POLA-02
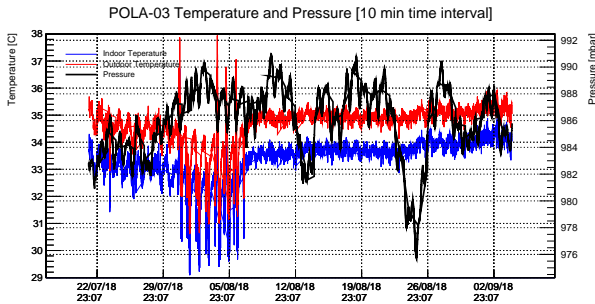


**(c)** POLA-03

**FIG. 2:** Temperature and pressure over time for the detectors



**FIG. 3:** Uncorrected raw rate over time for all three detectors.



**(a)** Computed          **(b)** From article
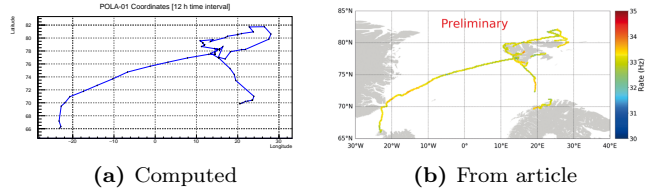
**FIG. 4:** a) Computed latitude and Longitude for the POLA-01 detector, both latitude and longitude is given in decimal coordinates. b) The voyage of Nanuq in longitude-latitude plane, displaying, in colour, the different preliminary rates measured by POLA-01, after pressure and vertical angle corrections-image from [2]

reasonable cuts on the data if any such points exsists. The raw rate for POLA-01 (black) and POLA-02 (red) overlap and are around the same range of values while the rate for POLA-03 is lower. This is explained in [2] as a result of the presence of dense material on the roof above the detector.For both POLA-02 and POLA-03 we can see a large deviation in pressure around 26/08/18, in this time period the raw rates also deviate quite alot.

## B.   Particle Raw Rate

The raw rate is defined as raw rate = NumEvents/time. In FIG. 3 this raw rate is plotted as a function of time for the three detectors. I have removed any outliers that will cause trouble later by applying

### 1.   Longitude and Latitude

The latitude and longitude of POLA-01 are shown in 4a. This can be compared to the image from the article [2] shown in FIG. 4b. FIG. 5 shows the raw rate as a function of longitude and latitude.
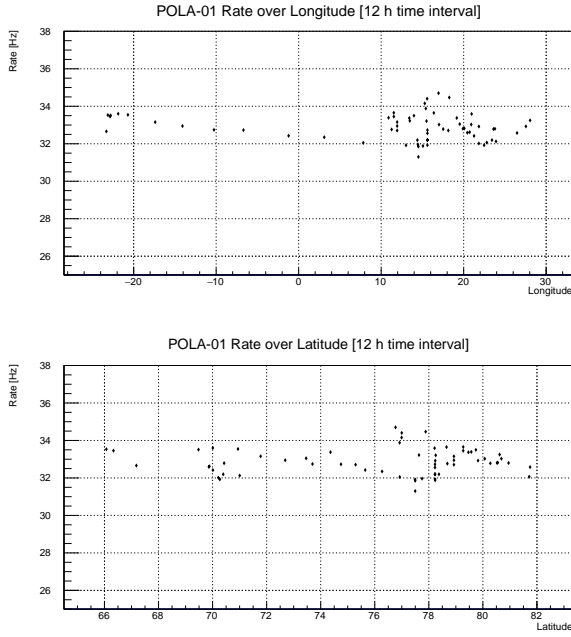
**FIG. 5:** Change in raw rate and longitude/latitude over time for POLA-01.

#### 2.   *Barometric Correction coefficients*

The change in rate caused by changes in the pressure is experimentally shown to have an exponential dependence which to first order approximation[3] [4] can be expressed as,

$$\frac{\Delta I}{I} \approx \beta \cdot \Delta P \tag{1}$$

where $\Delta P = P - P_ref$ and $\beta$ is the barometric coefficient. This coefficient is found by following the description from the EEE website [5] by plotting raw rate vs pressure and doing a linear fit to the data. The barometric coefficient is then

$$\beta = \frac{p1}{\text{avgRawRate}} \cdot 100[\%/\text{mbar}] \tag{2}$$

Once we find $\beta$ we retrieve the corrected rate using

$$\text{CorrectedRate} = \text{RawRate}(1 - \beta \Delta P) \tag{3}$$

To calculate the temperature coefficient $\alpha$, multiple methods are described by Berkova et. al in [6]. In this analysis no temperature correction is yet applied, so $\alpha = 0$.

#### 3.   *Pressure and Temperature*

In figures 8 the raw rate is plotted as a function on temperature and as a function of pressure. The barometric coefficient is found using EQ. 2, and listed in II along with the reference pressure for each detector. Within the uncertainty the barometric coefficients for POLA-01 and POLA-02 are the same, while for POLA-03, which was located in Italy, is significantly lower.

**TABLE II:** Barometric coefficients and reference pressure for the detectors.

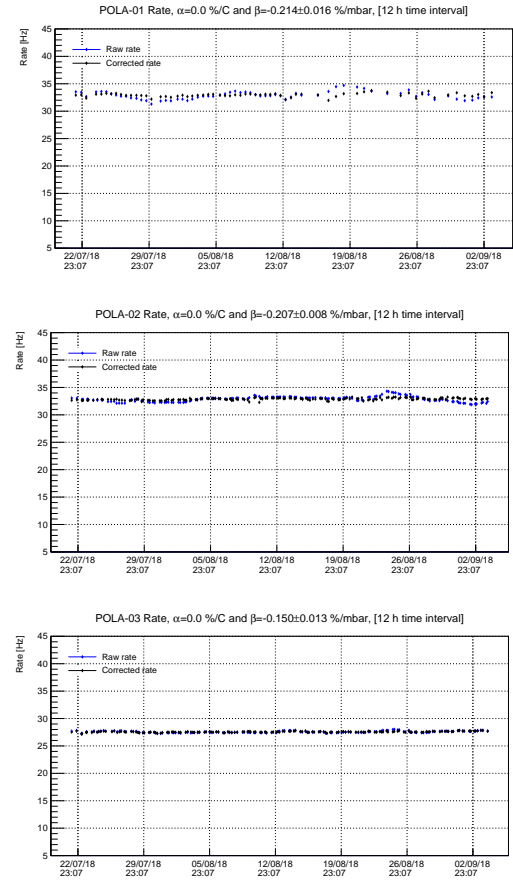|                  | POLA-01          | POLA-02            | POLA-03          |
|------------------|------------------|--------------------|------------------|
| $p_{\text{ref}}$[mbar] | 1011.85          | 1008.53            | 985.87           |
| $\beta$ [%/mbar] | $-0.25 \pm 0.02$ | $-0.207 \pm 0.008$ | $-0.15 \pm 0.01$ |







**FIG. 6:** Uncorrected and corrected rates for the tree detectors.

#### 4.   *Corrected Raw Rate*

Figures 6a-6c show the rates before and after using the pressure correction in EQ. 3. In figure 7 the corrected raw rate for all detectors are plotted together. There are still some small sudden deviations in the rates, so it may be necessary to apply a temperature correction for all three detectors, and in the case of POLA-01 a correction due to the detector orientation which may change when sailing.
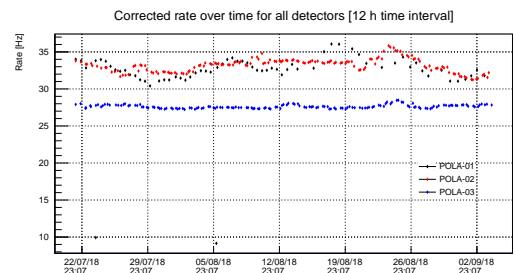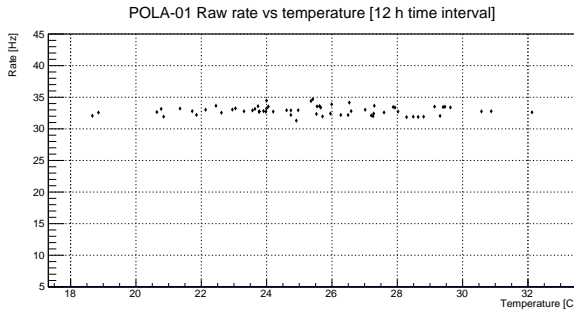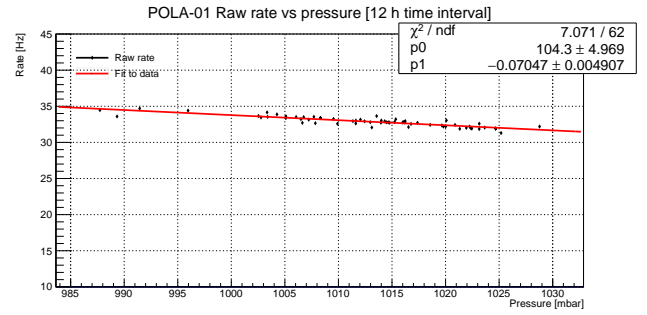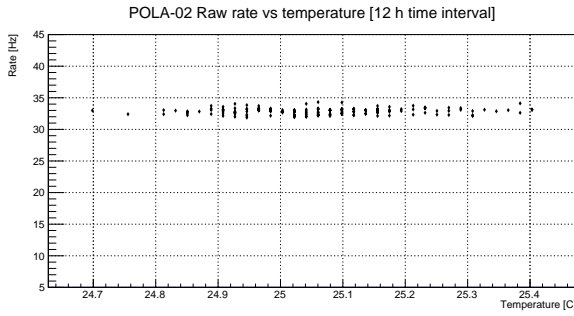


**FIG. 7:** Corrected rate for all three detectors.
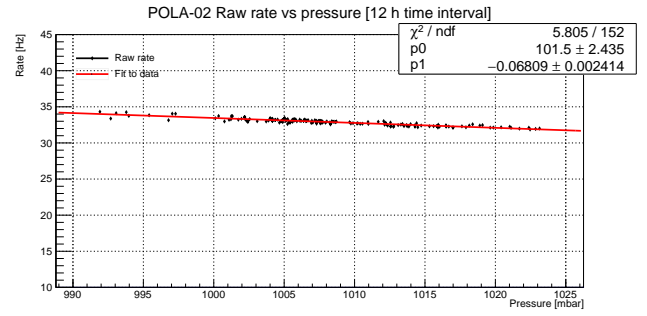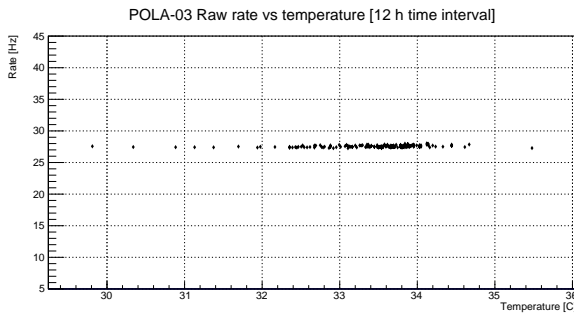
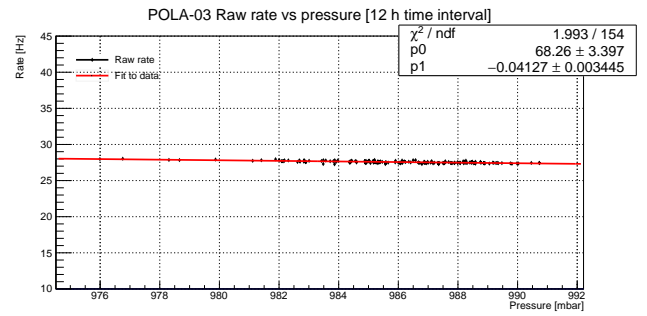**(a)** POLA-01



**(b)** POLA-01



**(c)** POLA-02



**(d)** POLA-02



**(e)** POLA-03



**(f)** POLA-03

**FIG. 8:** Plots on the left show the uncorrected raw rate as a function of temperature and on the right the uncorrected raw rate as a function of pressure. The red line shows the linear fit of the data.

[1] M. Tanabashi, K. Hagiwara, K. Hikasa, K. Nakamura, Y. Sumino, F. Takahashi, J. Tanaka, K. Agashe, G. Aielli, C. Amsler, M. Antonelli, D. M. Asner, H. Baer, Sw. Banerjee, R. M. Barnett, T. Basaglia, C. W. Bauer, J. J. Beatty, V. I. Belousov, J. Beringer, S. Bethke, A. Bettini, H. Bichsel, O. Biebel, K. M. Black, E. Blucher, O. Buchmuller, V. Burkert, M. A. Bychkov, R. N. Cahn, M. Carena, A. Ceccucci, A. Cerri, D. Chakraborty, M.-C. Chen, R. S. Chivukula, G. Cowan, O. Dahl, G. D'Ambrosio, T. Damour, D. de Florian, A. de Gouvêa, T. DeGrand, P. de Jong, G. Dissertori, B. A. Dobrescu, M. D'Onofrio, M. Doser, M. Drees, H. K. Dreiner, D. A. Dwyer, P. Eerola, S. Eidelman, J. Ellis, J. Erler, V. V. Ezhela, W. Fetscher, B. D. Fields, R. Firestone, B. Foster, A. Freitas, H. Gallagher, L. Garren, H.-J. Gerber, G. Gerbier, T. Gershon, Y. Gershtein, T. Gherghetta, A. A. Godizov, M. Goodman, C. Grab, A. V. Gritsan, C. Grojean, D. E. Groom, M. Grünewald, A. Gurtu, T. Gutsche, H. E. Haber, C. Hanhart, S. Hashimoto, Y. Hayato, K. G. Hayes, A. Hebecker, S. Heinemeyer, B. Heltsley, J. J. Hernández-Rey, J. Hisano, A. Höcker, J. Holder, A. Holtkamp, T. Hyodo, K. D. Irwin, K. F. Johnson, M. Kado, M. Karliner, U. F. Katz, S. R. Klein, E. Klempt, R. V. Kowalewski, F. Krauss, M. Kreps, B. Krusche, Yu. V. Kuyanov, Y. Kwon, O. Lahav, J. Laiho, J. Lesgourgues, A. Liddle, Z. Ligeti, C.-J. Lin, C. Lippmann, T. M. Liss, L. Littenberg, K. S. Lugovsky, S. B. Lugovsky, A. Lusiani, Y. Makida, F. Maltoni, T. Mannel, A. V. Manohar, W. J. Marciano, A. D. Martin, A. Masoni, J. Matthews, U.-G. Meißner, D. Milstead, R. E. Mitchell, K. Mönig, P. Molaro, F. Moortgat, M. Moskovic, H. Murayama, M. Narain, P. Nason, S. Navas, M. Neubert, P. Nevski, Y. Nir, K. A. Olive, S. Pagan Griso, J. Parsons, C. Patrignani, J. A. Peacock, M. Pennington, S. T. Petcov, V. A. Petrov, E. Pianori, A. Piepke, A. Pomarol, A. Quadt, J. Rademacker, G. Raffelt, B. N. Ratcliff, P. Richardson, A. Ringwald, S. Roesler, S. Rolli, A. Romaniouk, L. J. Rosenberg, J. L. Rosner, G. Rybka, R. A. Ryutin, C. T. Sachrajda, Y. Sakai, G. P. Salam, S. Sarkar, F. Sauli, O. Schneider, K. Scholberg, A. J. Schwartz, D. Scott, V. Sharma, S. R. Sharpe, T. Shutt, M. Silari, T. Sjöstrand, P. Skands, T. Skwarnicki, J. G. Smith, G. F. Smoot, S. Spanier, H. Spieler, C. Spiering, A. Stahl, S. L. Stone, T. Sumiyoshi, M. J. Syphers, K. Terashi, J. Terning, U. Thoma, R. S. Thorne, L. Tiator, M. Titov, N. P. Tkachenko, N. A. Törnqvist, D. R. Tovey, G. Valencia, R. Van de Water, N. Varelas, G. Venanzoni, L. Verde,

M. G. Vincter, P. Vogel, A. Vogt, S. P. Wakely, W. Walkowiak, C. W. Walter, D. Wands, D. R. Ward, M. O. Wascko, G. Weiglein, D. H. Weinberg, E. J. Weinberg, M. White, L. R. Wiencke, S. Willocq, C. G. Wohl, J. Womersley, C. L. Woody, R. L. Workman, W.-M. Yao, G. P. Zeller, O. V. Zenin, R.-Y. Zhu, S.-L. Zhu, F. Zimmermann, P. A. Zyla, J. Anderson, L. Fuller, V. S. Lugovsky, and P. Schaffner. Review of particle physics. *Phys. Rev. D*, 98:030001, Aug 2018. doi: 10.1103/PhysRevD.98.030001. URL https://link.aps.org/doi/10.1103/PhysRevD.98.030001.

[2] O. Pinazza R. Nania. Measuring cosmic ray showers with near the north pole with the extreme energy events project. *Il Nuovo Saggiatore*, 34(5-6), 2018. URL https://www.ilnuovosaggiatore.sif.it/article/179.

[3] Kobelev, A. Belov, E Mavromichalaki, M. Gerontidou, and Victor Yanke. Variations of barometric coefficients of the neutron component in the 22-23 cycles of solar activity. 01 2011.

[4] R. R. S. De Mendonça, J. P. Raulin, E. Echer, V. S. Makhmutov, and G. Fernandez. Analysis of atmospheric pressure and temperature effects on cosmic ray measurements. *Journal of Geophysical Research: Space Physics*, 118(4):1403–1409, 2013. doi: 10.1029/2012JA018026. URL https://agupubs.onlinelibrary.wiley.com/doi/abs/10.1029/2012JA018026.

[5] P.La Rocca and F.Riggi. Procedure for the determination of the barometric coefficient. URL https://eee.centrofermi.it/research/documents-and-procedures.

[6] M. Berkova, A. Belov, E. Eroshenko, and V. Yanke. Temperature effect of muon component and practical questions of how to take into account in real time. *Astrophysics and Space Sciences Transactions*, 8(1):41–44, 2012. doi: 10.5194/astra-8-41-2012. URL http://www.astrophys-space-sci-trans.net/8/41/2012/.